

Article

One Week Feeding of CDAHFD Induces Steatohepatitis and Mitochondrial Dysfunction with Oxidative Stress in Liver

Takehito Sugasawa ^{1,†}, Seiko Ono ^{2,†}, Masato Yonamine ^{1,†}, Shin-ichiro Fujita ¹, Yuki Matsumoto ³, Kai Aoki ^{1,4}, Takuro Nakano ², Shinsuke Tami ⁵, Yasuko Yoshida ^{1,6}, Yasushi Kawakami ¹ and Kazuhiro Takekoshi ^{1,*}

¹ Laboratory of Laboratory/Sports Medicine, Division of Clinical Medicine, Faculty of Medicine, University of Tsukuba, 1-1-1 Tennodai, Tsukuba 305-8577, Ibaraki, Japan; take0716@krf.biglobe.ne.jp (T.S.), yonamine.masato.fu@u.tsukuba.ac.jp (M.Y.), shin.ichiro.fujita.03@gmail.com (S.F.), fineday0126@gmail.com (K.A.), y-yoshida@tius.ac.jp (Y.Y.), y-kawa@md.tsukuba.ac.jp (Y.K.), k-takemd@md.tsukuba.ac.jp (K.T.)

² Master's Program in Medical Sciences, Graduate School of Comprehensive Human Sciences, University of Tsukuba, 1-1-1 Tennodai, Tsukuba 305-8577, Ibaraki, Japan; jimbeamilkybonbon330@gmail.com (S.O.), s2021408@s.tsukuba.ac.jp (T.N.)

³ Research and Development Section, Anicom Specialty Medical Institute Inc., 2-6-3 Chojamachi 5F, Yokohamashi-Nakaku, 231-0033, Kanagawa, Japan; ymatsumoto.ac@gmail.com (Y.M.)

⁴ Japan Society for the Promotion of Science; Kojimachi Business Center Building, Kojimachi, Chiyoda-ku, Tokyo 102-0083, Japan

⁵ Doctoral Program in Sports Medicine, Graduate School of Comprehensive Human Sciences, University of Tsukuba, 1-1-1 Tennodai, Tsukuba, Ibaraki 305-8577, Japan; tama1994@outlook.jp (S.T.)

⁶ Department of Medical Technology, Faculty of Health Sciences, Tsukuba International University, 6-20-1 Manabe, Tsuchiura, Ibaraki 300-0051, Japan

* Correspondence: k-takemd@md.tsukuba.ac.jp; Tel.: +81-29-853-3209

† These authors contributed equally to this work.

Abstract: The prevalence of nonalcoholic fatty liver disease (NAFLD) has been rapidly increasing worldwide. A choline-deficient L-amino acid-defined high fat diet (CDHFD) has been used to create a mouse model of nonalcoholic steatohepatitis (NASH). There are some reports about the effects on mice of being fed CDAHFD for a long time, 1 to 3 months. However, the effect of this diet over a short period has been unknown. Therefore, we examined the effect of one week of feeding CDAHFD on the mouse liver. Feeding this diet for only one week induced lipid droplet deposition in the liver with increasing activity of liver-derived enzymes in the plasma. On the other hand, it did not induce fibrosis and cirrhosis. Additionally, it was demonstrated that mitochondrial respiration is significantly impaired with severe oxidative stress in the liver by CDAHFD, associated with a decreasing mitochondrial DNA copy number and complexes-proteins. In the gene expression analysis of the liver, inflammatory and oxidative stress markers were significantly increased by CDAHFD. These results demonstrated that one week of feeding CDAHFD to mice induces steatohepatitis with mitochondrial dysfunction and severe oxidative stress, without fibrosis, which can partially mimic the early stage of the NASH in humans.

Keywords: CDAHFD; NASH; Mitochondrial dysfunction; Liver; Oxidative Stress

1. Introduction

Nonalcoholic fatty liver disease (NAFLD) includes simple steatosis (nonalcoholic fatty liver: NAFL) and nonalcoholic steatohepatitis (NASH); NASH can be progressive and predisposes individuals to the development of fibrosis and cancer [1]. Also, unlike other organs, it is well known that many types of liver damage, such as simple steatosis, steatohepatitis, and fibrosis, are unlikely to cause specific subjective symptoms, although the patients may have systematic symptoms that are non-specific to the damage [2,3]. Additionally, NAFLD is rapidly becoming the most common cause of chronic liver disease due to an increase in the prevalence of obesity [4] in recent years. For the same reason, the incidence and prevalence of NAFLD is rapidly increasing worldwide [1]. Therefore, the development of new treatments has become urgent, in particular, therapeutic medicines

that can be used to treat patients who have early-stage NAFLD. However, no medicines have been approved to treat NAFLD at present [5].

There are many studies using animal models of NAFLD to develop new treatments and to investigate its molecular mechanisms. In general, the NAFLD model is created by feeding an unbalanced diet, such as a high-fat diet (HFD) [6-8], a high-fat high-sucrose diet (HS-HFD) [9, 10], or a high-fat, high-cholesterol diet [11, 12]. Moreover, NASH models including fibrosis and steatohepatitis have made using a choline-deficient, L-amino acid-defined, high-fat diet (CDAHFD) [13-16]. The duration of the animal experiments using the various models mentioned above was the long term, from 8 to 12 weeks or longer [6-16]. Such long-term experiments can sometimes be a major impediment to the progress of research, as it takes a very long time to obtain results. In addition, most public grants are time-limited, and the researcher must complete the experiment as soon as possible and move on to the next steps. Considering these factors, animal models that can save time are extremely valuable because they accelerate research.

Given that CDAHFD progresses faster to liver steatosis than an HFD, it can be used to create a more severe steatohepatitis with fibrosis (NSHA with fibrosis) model of the liver. This is because the formulation of the diet as choline-deficient, L-amino acid-defined restricts the secretion of triglyceride into the blood from the liver. Therefore, we hypothesized that even a short feeding period, such as one week, may induce simple fatty liver or steatohepatitis that resembles NAFL or NASH. Furthermore, in our experience, we have observed a sufficiently fatty liver after only one week of feeding CDAHFD. In addition, there is no report with a detailed analysis at the molecular level of the liver after one week feeding of this diet so far, and the influences of the diet are unknown.

Therefore, this study aimed to investigate and clarify the influence of one week feeding of CDAHFD on the liver in detail. Moreover, we focused not only on parameters that reflect a fatty liver, but also on parameters of inflammation, mitochondrial dysfunction and oxidative stress, because these 3 parameters are strongly associated with the progression of the disease state in NAFLD [17-19] as the 2nd hit theory [20, 21].

We observed similar pathology to early stage NASH without fibrosis in the model. Moreover, we provided several and important evaluation methods of the model to researchers in this field. Therefore, these achievements would be expected to accelerate the research progress.

2. Results

2.1. Phenotypic analyses showed significant changes in the liver in the CDAHFD group.

The overview of this animal experiment is shown in Figure 1A. Seven-week-old mice were randomly assigned to 3 groups to feed a normal diet (ND; N=12), an HFD (N=12) or a CDAHFD (N=13) for a week. In the results, exterior photographs of the liver at dissection showed significant changes of brown-red to brown-white in the CDAHFD group (Figure 1B), which may reflect lipid accumulation. Food intake (kcal)/cage/week was a little higher on HFD and CDAHFD compared to the ND group (Figure 1C). On the other hand, body weight was slightly increased in the HFD group only (Figure 1D). Blood glucose in the fasting condition for 5 hours was significantly decreased in the CDAHFD group compared to the other 2 groups (Figure 1E). The liver weight and liver/body weight were slightly increased in the CDAHFD group compared with the other 2 groups (Figure 1F and G). On the other hand, the amount of triglyceride (TG) in the liver tissue was drastically increased in the CDAHFD group, approximately 100-fold higher compared to the other 2 groups. These results suggested that one-week feeding of CDAHFD is successful in establishing the early-stage NASH model and the CDAHFD group can develop a severe fatty liver even though their blood glucose is decreased.

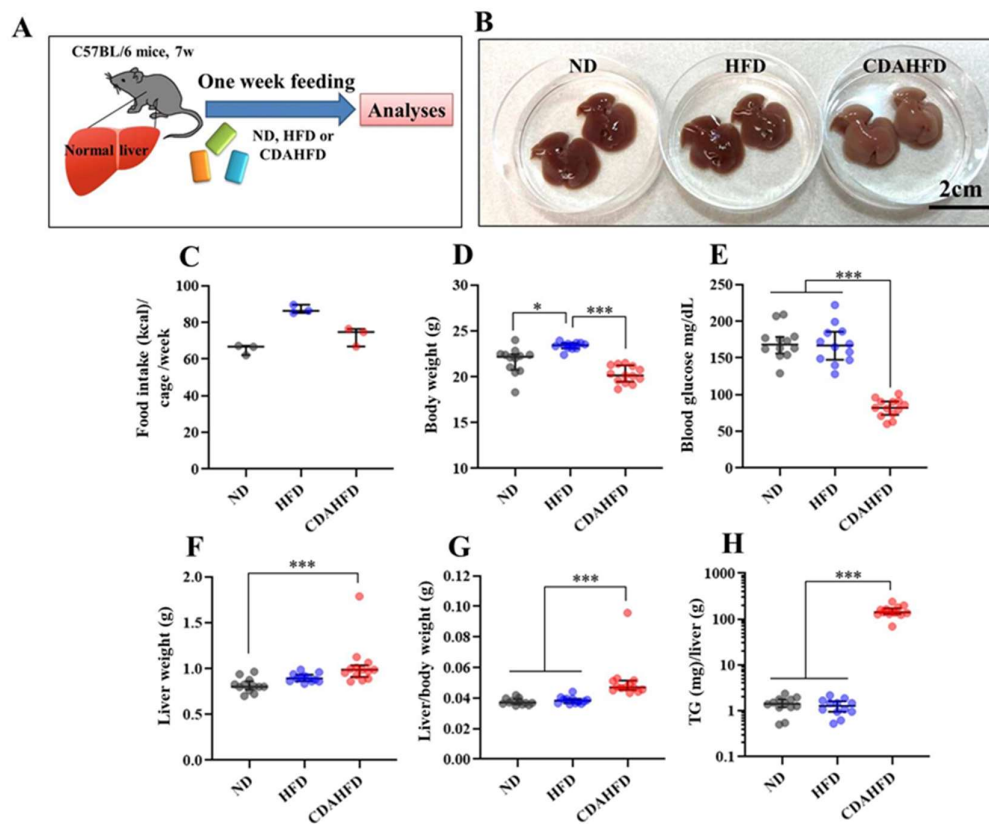


Figure 1. Results of the phenotypic analyses. A: Overview of this animal experiment, B: exterior photographs of the liver of representative samples in each group, C: food intake (kcal)/cage/week, each group had 3 cages (3 plot) including 3-5 mice each, D: body weight (g), E: blood glucose (mg/dL), F: liver weight (g), G: liver/body weight (g), H: TG (mg)/liver (g). * $p < 0.05$, *** $p < 0.001$, respectively.

2.2. CDAHFD generated lipid droplets in the liver with an inflammatory response

Tissue slides of formalin-fixed paraffin-embedded (FFPE) samples subjected to staining and morphologic analyses were created using randomly selected 7 samples from each group. The results of the tissue staining are shown in Figure 2A. In the hematoxylin-eosin (HE) and Masson's trichrome (MT) staining, many lipid droplets were observed in the CDAHFD group (Figure 2A-HE and MT staining). Supporting these observations, the lipid droplet areas (%) on the HE stained slides were drastically increased in the CDAHFD group compared to the other 2 groups (Figure 2B). On the other hand, no fibrosis was observed by MT staining (Figure 2A-MT staining).

As shown by the arrowheads, cell accumulations were often observed in the CDAHFD group on the HE staining. The asterisk site is magnified on the right side, and the accumulated cells appeared to be inflammatory cells, such as neutrophils that have a characteristic morphology with a lobed nucleus (Figure 2A-HE staining). In support of these observations, immunofluorescence (IF) staining revealed the localization of myeloperoxidase at the cell accumulation site (Figure 2A-IF stain). In other words, it can be concluded that neutrophils are the main component of the cell accumulations.

In addition, the degrees of pathological progression were evaluated using the Steatosis, Activity and Fibrosis (SAF) scoring system [22]. The results indicated that all samples in the CDAHFD group were score 4 (steatosis: 1, portal inflammation: 2, ballooning: 1, and fibrosis: 0 in all samples), and all samples in the other 2 groups were score 0.

These results suggest that one week of feeding CDAHFD induces the deposition of lipid droplets with infiltration of inflammatory cells, without fibrosis.

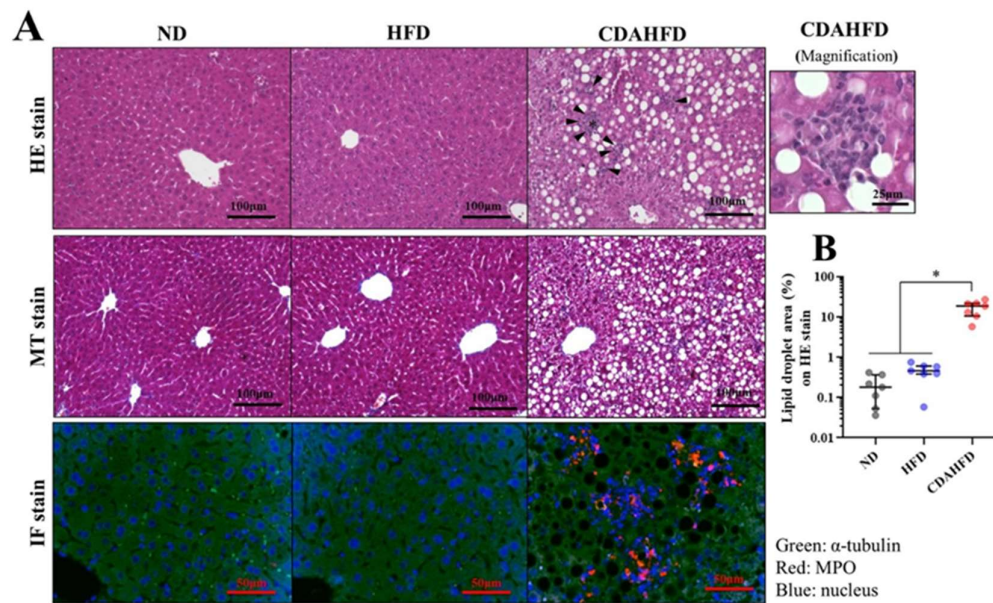


Figure 2. Morphological observation of the liver after ND, HFD or CDAHFD. A: HE, MT and IF staining for the liver in each group. The site of cell accumulation observed on HE staining is individually magnified in the right figure. B: quantification of lipid droplet area on HE stain in each group. * $p < 0.05$.

2.3. CDAHFD induced increasing liver deviation-enzyme activities in the plasma

General biomarkers were measured in the plasma from the mice. The activities of aspartate transaminase (AST) and alanine aminotransferase (ALT) were significantly increased in the CDAHFD group compared to the other 2 groups (Figure 3A and B). Particularly, the ALT activity of the CDAHFD group was 14 to 16-fold higher than in the other 2 groups (Figure 3B). Plasma TG was slightly decreased in the CDAHFD group compared to the control group (Figure 3C). Non-esterified free fatty acid (NEFFA) was not changed (Figure 3D). Total cholesterol (T-CHO), low/high-density lipoprotein cholesterol (HDL/LDL) was significantly decreased in the CDAHFD group compared to the other groups. On the other hand, T-CHO and HDL were significantly increased in the HFD group compared to the other 2 groups (Figure 3E and F). These results suggest that one week feeding of CDAHFD rapidly induced liver damage even though the plasma cholesterol was decreased.

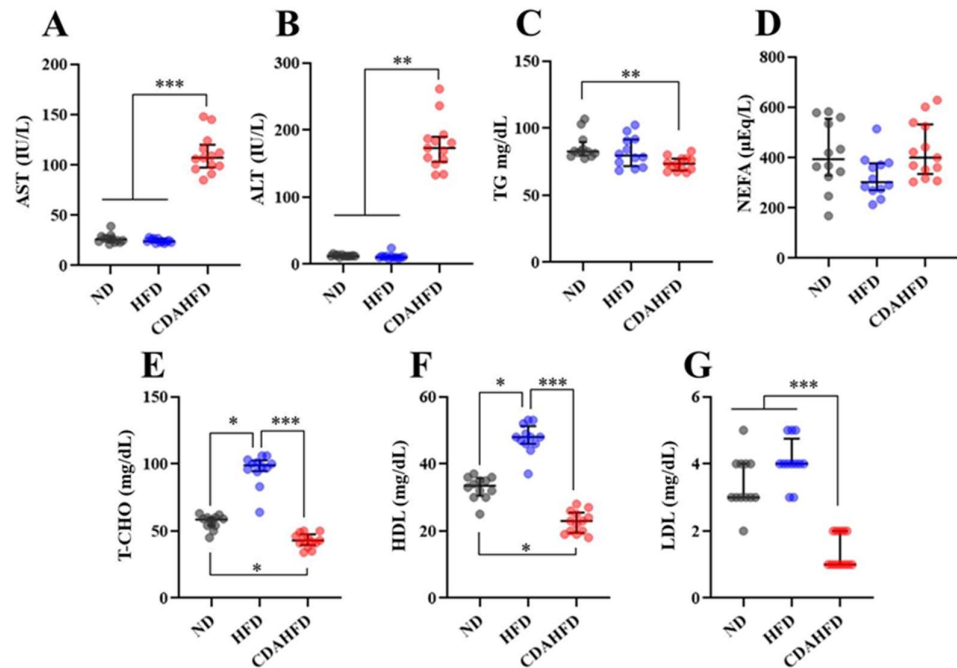


Figure 3. Measurements of the general biomarkers in the plasma. A: AST (IU/L), B: ALT (IU/L), C: TG (mg/dL), D: NEFA (μ Eq/L), E: T-CHO (mg/dL), F: HDL (mg/dL), G: LDL (mg/dL). * $p < 0.05$, ** $p < 0.01$, *** $p < 0.001$, respectively.

2.4. CDAHFD induced increasing oxidative stress and mitochondrial dysfunction in the liver

Oxidative stress markers, antioxidant enzyme activity, mitochondrial activity, and DNA copy number were measured in the liver tissue. In the results, thiobarbituric acid reactive substance (TBARS) and dichlorofluorescein (DCF), a parameter of lipid peroxidation and reactive oxygen species, were significantly increased in the CDAHFD group compared to the other 2 groups (Figure 4A and B). Particularly, the TBARS in the CDAHFD group were 23 to 26-fold higher than in the other 2 groups (Figure 4A). On the other hand, catalase (CAT) and superoxide dismutase, as a first-line antioxidants, were significantly decreased in the CDAHFD group compared to the other 2 groups (Figure 4C and D). Also, Resazurin and JC-1 assays, which can reflect mitochondrial activity, indicated significantly or marginally decreased activity in the CDAHFD group compared to the other 2 groups (Figure 4E and F). Consistent with this finding, mitochondrial DNA (mtDNA) copy numbers in the mitochondrial fraction and whole liver were significantly decreased (Figure 4G and H). These results suggested that one week feeding of CDAHFD induced increasing oxidative stress and mitochondrial dysfunction with decreased antioxidants in the liver and inflicting damage on the mitochondria by lipid peroxidation reaction, reaching a severe state.

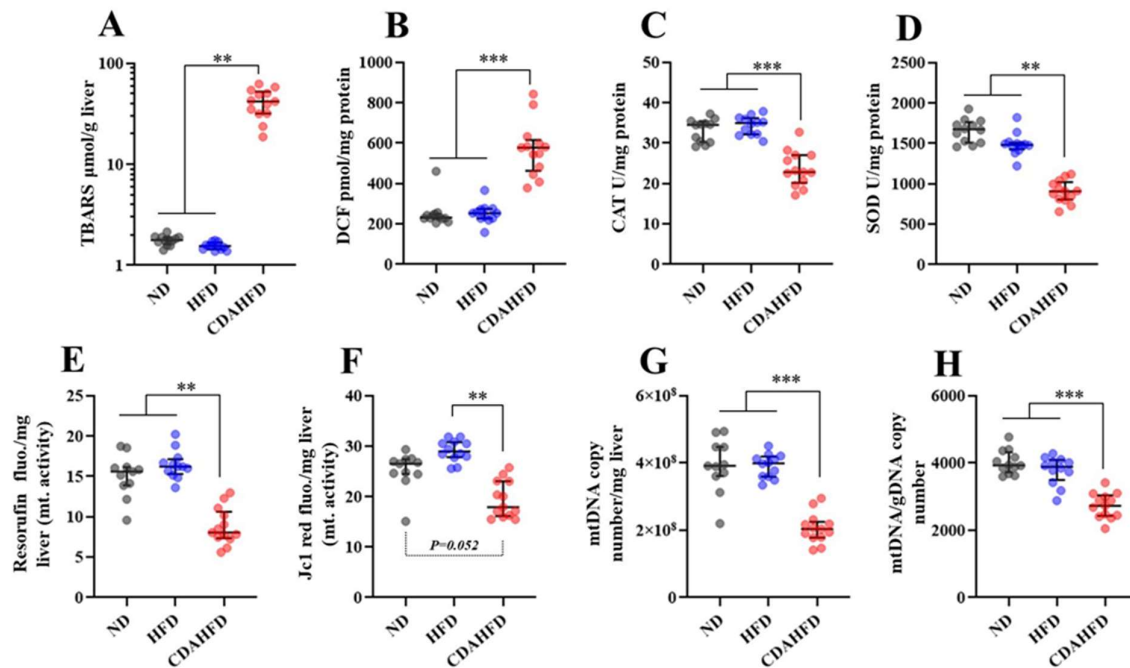


Figure 4. Measurements of the oxidative stress markers, antioxidant activities, and mitochondrial activities and copy numbers in the liver tissue. A: TBARS ($\mu\text{mol/g}$ liver), B: DCF (pmol/mg protein), C: CAT activities (U/mg protein), D: SOD activities (U/mg protein), E: Resorufin fluorescence/mg liver of the Resazurin assay that can measure mitochondrial activity, F: JC-1 red fluorescence mg liver of the JC-1 assay that can also measure mitochondrial activity, G: mtDNA copy numbers/mg liver in the mitochondrial fraction, H: mtDNA/gDNA copy number in whole liver tissue. ** $p < 0.01$, *** $p < 0.001$, respectively.

2.5. CDAHFD induced decreasing mitochondrial proteins and increasing NRF2 target proteins in the liver.

Oxidative phosphorylation (OXPHOS) proteins (complex proteins) and other constituent proteins in the mitochondria were quantified using an isolated mitochondrial fraction in western blot (WB) analysis. Nuclear factor erythroid 2-related factor 2 (NRF2) target proteins were also quantified using whole liver protein, which reflects oxidative stress. In the blot data on Figure 5A that show representative samples with $N=4$ in each group, it seemed that OXPHOS and other constituent proteins in the mitochondria were decreased. Supporting this, the quantitative values of the protein expression levels of OXPHOS and other constituent proteins of the mitochondria in all samples were significantly decreased in the CDAHFD group compared to the other 2 groups (Figure 5B and C). In the blot data in Figure 5D, it seemed that NRF2 target proteins were increased. Supporting this, the quantitative values of NRF2, NQO1, and HO1 in all of the samples were significantly increased compared to the other 2 groups (Figure 5E and F). These results suggest that one week feeding of CDAHFD induced decreases in the expression of mitochondrial proteins with activation of NRFs by oxidative stress.

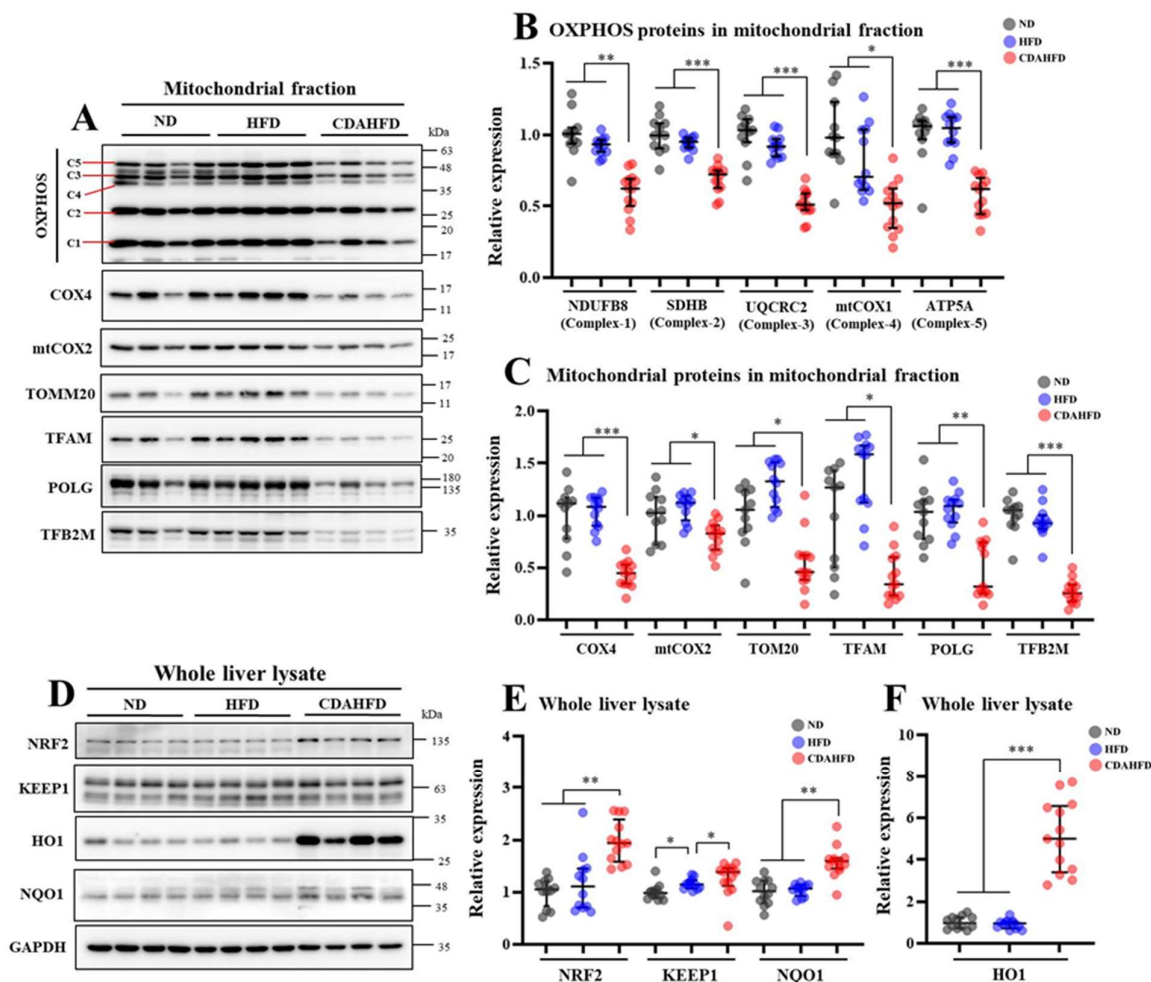


Figure 5. Measurements of mitochondrial proteins in the mitochondrial fraction and NRF2 target proteins in the whole liver lysate on WB analysis. A: Representative blot data of mitochondrial proteins in an isolated mitochondrial fraction as N=4 in each group, C1-5 mean mitochondrial complex 1-5, B: relative protein expression in the quantified results for the band of OXPHOS protein in all of the samples, C: relative protein expression in the quantified results for the bands of the other mitochondrial proteins for all of the samples, D: representative blot data of NRF2 target proteins in whole liver lysate as N=4 on each group, E and F: relative protein expression in quantified results for the band of NRF2 for all samples. * $p < 0.05$, ** $p < 0.01$, *** $p < 0.001$, respectively.

2.6. CDAHFD modified gene expression patterns about inflammation, fibrosis, oxidative stress, lipogenesis and gluconeogenesis in the liver, with upregulated inflammatory marker genes in the whole blood.

The expression of genes involved in the inflammatory response were measured in the whole blood. *Il1- β* and *Lcn2*, reflecting the acute inflammatory response, were significantly increased in the CDAHFD group compared to the other groups, although the expression of *Tnf- α* was not changed (Figure 6A). The gene expression of each marker gene for inflammation, cell growth, fibrosis, antioxidant enzymes, NRF2 target genes (response to oxidative stress), lipogenesis, and gluconeogenesis were measured using liver tissues. The inflammation marker genes such as *Tnf- α* , *Mcp1* and *Lcn2* were drastically increased in the CDAHFD group compared to the other 2 groups (Figure 6B). Particularly, *Lcn2* was the most increased by 182-fold in the CDAHFD group compared to the ND group (Figure 6A). In the cell growth markers, gene expression of *Ki67* was significantly increased in the CDAHFD group compared to the other 2 groups (Figure 6C). In the cell fibrosis markers,

gene expression of *Col1a1* and *Col3a1* were significantly increased in the CDAHFD group compared to the other 2 groups (Figure 6D). In the markers of antioxidant enzymes, gene expression of *Gpx2*, *Cat* and *Sod3* were significantly decreased in the CDAHFD group compared to the other 2 groups. Gene expression of *Gpx1* was decreased in the CDAHFD group compared to the only ND group. Gene expression of *Sod1* and *Sod2* were decreased in the CDAHFD group compared to the HFD group (Figure 6E); when integrated analyses for *Sod1* and 2 in each group were performed, the values were significantly decreased in the CDAHFD group compared to the other 2 groups even though they were significantly increased in the HFD group compared to the other 2 groups (Supplementary Figure S1). In the NRF2 target genes, gene expression of *Nqo1* and *Ho1* were significantly increased in the CDAHFD group compared to the other 2 groups, although *Nrf2* was increased in the HFD group compared to the other 2 groups (Figure 6F). In the marker genes of lipogenesis, gene expression of *Scd1*, *Fasn*, and *Srebf-1c* were significantly decreased in the CDAHFD group compared to the other 2 groups (Figure 6G). Particularly, *Scd1* was drastically decreased -151-fold in the CDAHFD group compared to the ND group (Figure 6G). On the other hand, gene expression of *Ppar γ* and *Srebf-1a* were not changed between the ND and CDAHFD groups (Figure 6G). In the marker genes of gluconeogenesis, gene expression of *G6pc* and *Pepck* were significantly decreased in the CDAHFD group compared with the other 2 groups (Figure 6G). From these results, CDAHFD appears to induce the following response in the liver with severe inflammation, increased fibrosis, decreased antioxidant enzymes, increased oxidative stress, decreased de novo lipogenesis, and decreased gluconeogenesis.

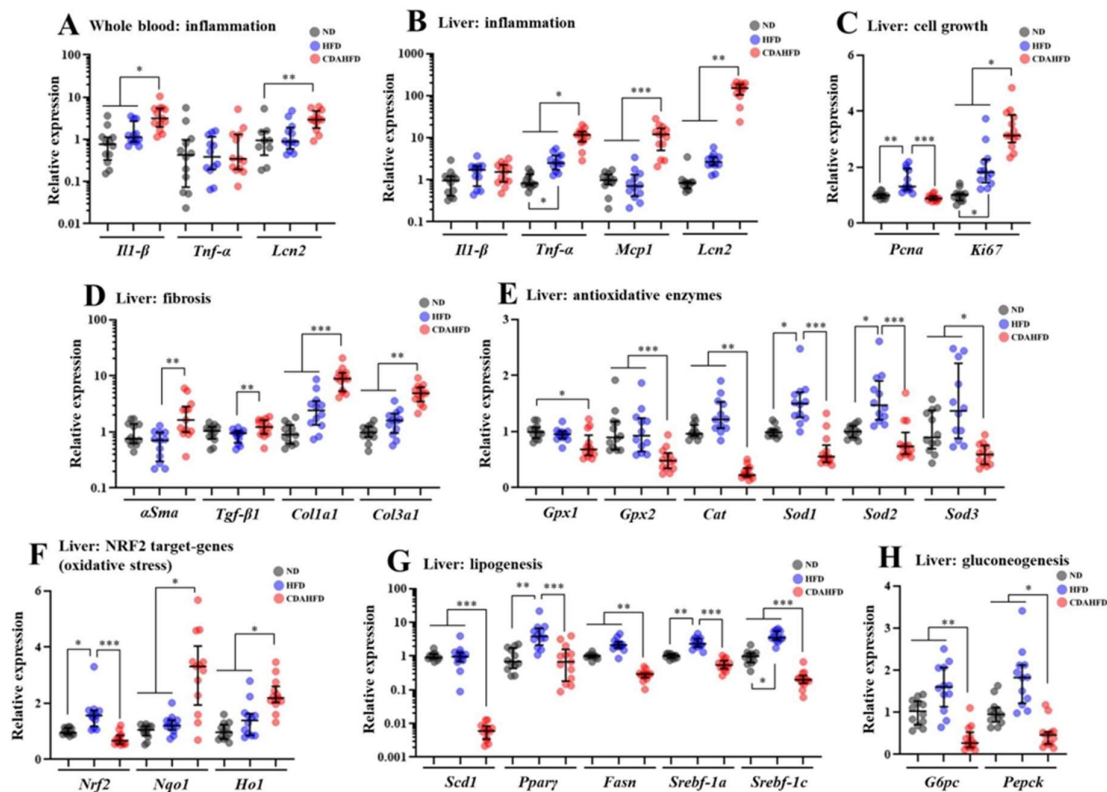


Figure 6. Quantification of gene expression for the several marker genes in the whole blood and liver. The types of samples are whole blood (A) and liver (B-H). A: inflammatory markers in the whole blood, B: inflammatory markers in the liver, C: cell growth markers in the liver, D: fibrosis markers in the liver, E: antioxidative enzymes in the liver, F: NRF2 target genes in the liver, G: lipogenesis markers in the liver, H: gluconeogenesis markers in the liver. * $p < 0.05$, ** $p < 0.01$, *** $p < 0.001$, respectively.

3. Discussion

The number of patients affected by NAFLD (including NASH) has been rapidly increasing worldwide and it predisposes individuals to fibrosis and liver cancer development [1]. Therefore, it is important to understand the molecular mechanism of NAFLD, including NASH, to develop new treatments. In particular, understanding the stage of NASH before the development of fibrosis can be useful in stopping its progression to irreversible NAFLD. Therefore, we established a model of early-stage NASH by feeding mice CDAHFD for one week. The mice developed liver damage with severe hepatic steatosis and elevated hepatic triglycerides, associated with elevated liver damage markers in the plasma. On the other hand, the mice with HFD feeding were not observed to have liver damage, lipid deposition, etc. Furthermore, we confirmed that the inflammatory response and oxidative stress in the liver were significantly increased in only the CDAHFD group. In particular, lipid peroxidation was drastically increased upon feeding CDAHFD for one week. Additionally, our results showed that the mitochondrial function and mitochondrial numbers and proteins in the liver were significantly decreased in the CDAHFD group, suggesting that the mitochondria suffer severe damage; this phenomenon is also similar to that observed in NASH patients [23].

In this way, we observed severe damage with mitochondrial dysfunction in the liver in this model. On the other hand, the pathological findings showed no fibrosis, even though gene expression of fibrosis markers was significantly increased. Given the above in an integrated manner, it is possible that the NASH model could be established in only one week; and this model is before fibrosis develops, with inflammation, oxidative stress, and mitochondrial damage.

We also performed a human-adapted pathological examination for the liver in this model. The Steatosis, Activity and Fibrosis (SAF) scoring system has been globally used as an indicator for assessing the progression in the liver of NAFLD on clinical examinations of humans. The SAF score can indicate steatosis, lobular inflammation, portal inflammation, ballooning and fibrosis [22] using pathological specimens. Also, this scoring system can be applied to animal models of NAFLD [24]. Therefore, in this study, we also applied the SAF scoring system for the pathological specimens of the model. The results showed that all samples in the CDAHFD group were score 4 (steatosis: 1, portal inflammation: 2, ballooning: 1, and fibrosis: 0 in all samples). On the other hand, all samples in the other 2 groups were score 0. The SAF score of the CDAHFD fed group proves that the liver phenotype of this model is not simple steatosis (NAFL), but active and progressive NASH [22]. Histological activity in SAF scores is also known to be related to the severity of fibrosis [25]. Therefore, it can be judged that the pathological condition of this model is NASH without fibrosis with active and progressive advancement of the pathology. In this way, even when the pathological specimen of this model is evaluated in the same way as clinical examinations for humans, it can be strongly judged to be early NASH without fibrosis, supporting the results of the other assays.

This model, which is created in just one week, would be very useful in studies of NAFLD, including NASH. If researchers select this model, they can save a lot of time on NAFLD research. Many studies using NAFLD models have reported requiring long-term feeding periods of 8 to 12 or more weeks [6-12] to establish the model, which means severe time loss. On the other hand, this model progresses in pathology faster than normal HFD even though it is able to be established faster, so if researchers want to develop a drug with this model, they may need a stronger efficacy. Therefore, researchers may need to fully understand the characteristics of each model before conducting experiments. In summary, the main feature of this model is to be an early stage model of NASH without fibrosis. Therefore, this model would be useful to establish a therapeutic strategy before the condition causes fibrosis.

The progression of pathogenesis in NAFLD, including NASH, at the cellular level focused on mitochondria has been understood as follows. Fatty acid accumulation is occurring due to an increase in the influx of fatty acids into the liver by excessive dietary fat [26]. Then, excessive flux of fatty acids into the mitochondria of the hepatocytes induces excessive oxidative stress, followed by oxidative stress that leads to apoptosis and necrosis

of the cells [26]. When mitochondria experience damage, it is known that mitochondrial activity and ATP synthesis are attenuated [27]. Additionally, excessive oxidative stress causes necrotic inflammation of hepatocytes [28]. Phenomena that are consistent with the above mentioned mechanisms were observed in our model as follows. The intensities of the Resorufin and JC-1-red fluorescence, which can reflect mitochondrial activity and number, were significantly decreased in the liver in the CDAHFD group compared to the other 2 groups. Additionally, the mitochondrial complex and components and the mitochondrial DNA copy number were also significantly decreased in the liver of the CDAHFD group. Moreover, the gene expression of inflammatory markers, particularly neutrophil markers indicating acute inflammation, were drastically increased in the liver of the CDAHFD group, and we also observed neutrophil infiltration and accumulation on the pathological specimens. Therefore, we can explain that our model of one week-CDAHFD feeding suffers mitochondrial damage with excessive fatty acid flux to the mitochondria, accompanied by severe oxidative stress and necrotic inflammation to the hepatocytes, forming a vicious cycle. Taken together with the mechanisms of NAFLD and the results of our experiments, it can be declared that our model has the same pathogenesis of NAFLD. Speculating from these results, the hepatocytes in the CDAHFD group may suffer energy metabolism disability with disrupted ATP production; therefore, the hepatocytes may be entering a further vicious cycle due to ATP depletion. However, this study did not focus on ATP production. Measuring the amount of ATP produced in liver tissue would also be important parameter to evaluate when conducting experiments using this model.

Antioxidant dynamics are also considered an important parameter in NAFLD because previous studies of NAFLD patients revealed that the activities of some antioxidant enzymes were significantly decreased in the liver of these patients, with increased oxidative stress [29]. Our results indicated that parameters reflecting oxidative stresses such as TBARS and DCF were significantly increased in the liver of the CDAHFD group compared to the other 2 groups. On the other hand, gene expression of *Gpxs* (glutathione peroxidases), *Cat* (catalase), and *Sods* (superoxide dismutases) were significantly decreased in the CDAHFD group, while the protein and gene expression of *Ho1* (hemo oxygenase 1), an antioxidant enzyme that is an NFR2 target, were significantly increased in the CDAHFD group compared to the other 2 groups.

In measurements of the enzyme activity of the liver, CAT and SOD activities in the liver were significantly decreased in the CDAHFD group. GPX, SOD and CAT play a very important role as antioxidants in the first line of defense against reactive oxygen species (ROS) to prevent oxidative stress [30]. Therefore, it can be considered that the antioxidant capacity in the liver was significantly impaired in the CDAHFD group, associated with drastically increased lipid peroxidation, and this canceled the antioxidant effect of the HO1. In addition, these results of the model are consistent with results of analyses in clinical samples of human liver [29]. Therefore, because the model has similar phenomenon of the dynamics of antioxidants in the liver of human NAFLD, it can be recognized as an important reason for explaining the usefulness of this model. Although the enzyme activity of GPX was not measured in this study, it can be strongly inferred that it will be a useful evaluation parameter when using this model. In future studies, it is strongly recommended to also measure the enzymatic activity of GPX.

It has been reported that NASH patients suffer mitochondrial dysfunction associated with decreasing enzyme activities of mitochondria respiratory chain (MRC) complexes (also called the OXPHOS protein) in liver [23]. Moreover, several review articles have supported the existence of mitochondrial dysfunction in NASH patients [31-33]. An abnormality of the mitochondria causes decreases in function and the components of the respiratory chain complex and electron transfer efficiency, resulting in increased ROS generation, which causes oxidative stress [23, 34]. In addition, the oxidative stress causes mitochondrial damage [33, 35]. Therefore, maintaining or amplifying mitochondrial function along with a defense against oxidative stress may be beneficial as a treatment for NASH patients. In this study, we established a NASH model mouse with accompanying

mitochondrial dysfunction and severe oxidative stress, which mimics the NASH condition in humans. We also established an evaluation method of the characteristics of the model. Therefore, this model and the evaluation methods in this study can be expected to be useful for the development of new treatments for humans, focusing on antioxidants and the maintenance of mitochondrial function. For example, applying compounds with antioxidant and mitochondrial activation ability to this model, such as resveratrol [36] or other polyphenols [37], would accelerate the development of a new treatment.

It is known that the occurrence of NAFLD in humans is strongly associated with obese and diabetic patients [38, 39]. A high body mass index (BMI; kg/m²), fat mass, and HOMA-IR (insulin resistance index assessed by homeostasis model assessment) were observed in NAFLD patients [23, 40]. In addition, plasma parameters such as ALT, AST, glucose, and TG were also high in the NAFLD patients [40, 41]. Moreover, the total VLDL-TG secretion rate from the liver is increased in these patients [42]. On the other hand, their plasma T-CHO, LDL and HDL are normal or only show slight changes [40, 41]. There are some inconsistencies when integrating these human clinical pathologies with the characteristics of this model. In the model fed CDAHFD for one week, body weight was not changed compared to the ND group; and plasma TG, glucose, T-CHO, HDL, and LDL were decreased in the model, which is consistent with previous research reported by Tasuda D. et al. [43]; because the blood glucose level was low in the model, insulin resistance did not occur. These findings are different from the clinical pathology of NAFLD, which means limitations of this model. Mice fed CDAHFD are unable to secrete TG and cholesterol from the liver, due to a failure of lipoprotein synthesis by choline deficiency and reduced methionine [44]; therefore, there is decreased T-CHO, HDL and LDL in the plasma in this model. Hence, researchers would be needed to consider these inconsistencies and mechanisms when using this model. Also, as mentioned earlier, this model showed decreased blood glucose levels. In the qPCR assay, gene expression of *G6pc* and *Pepck*, that is, gluconeogenesis markers, were significantly decreased in the model, which is consistent with the decreased blood glucose level. Inflammation and oxidative stress during obesity and type 2 diabetes are generally considered to be factors that upregulate gluconeogenesis [45, 46]. Therefore, to reveal the mechanisms of a decreased blood glucose level in the model, further analysis in detail is required focusing on the signaling pathway and metabolite profiling for gluconeogenesis in hepatocytes.

3. Conclusion

In summary, we were able to establish an early-stage NASH model without fibrosis after one week feeding of CDAHFD, which can partially mimic the condition of NASH. Our results can provide a tool to support taking a step forward to reveal the mechanisms and treatments of irreversible NASH in the early stage. Moreover, our results have provided several important evaluation methods of this model to researchers in this field, which would accelerate the research progress.

4. Materials and Methods

4.1. Animal experiments

All animal experiments in this study were approved by the Animal Care Committee, University of Tsukuba (approval number: 20-133). Five-week-old C57/B6J male mice were purchased from the Central Laboratories for Experimental Animals (Tokyo, Japan) and then subjected to a 2 week acclimation period. The mice were bred and maintained in an air-conditioned animal house under specific-pathogen-free (SPF) conditions and subjected to a 12/12 h light and dark cycle. The mice were fed standard mouse pellets and water ad libitum during the acclimation period. At the start of the experiments, the ages of the mice were 7 weeks. Also, 3 types of diets ND (Cat#MF; Oriental Yeast, Itabashi, Tokyo, Japan), HFD (Cat#D12492, 60 kcal% fat; Research Diets, New Brunswick, NJ, USA) and CDAHFD (Cat#A06071302, 60 kcal% fat with 0.1% methionine and no added choline;

Research Diets) were used in this experiment. An overview of the animal protocols of these experiments is shown in Figure 1A.

After the acclimation period, the mice were randomly assigned to 3 groups to be fed ND (N=12), HFD (N=12) or CDAHFD (N=13). The mice were kept at 4-5 mice/cage, 3 cages in each group. Each diet was given at 40 g/mouse for one week. After one week from the start of feeding, the mice were fasted for 5 hours, and then the blood glucose was measured using whole blood from the tail tip. The body weight and food intake were also measured at the same time. After that, the mice were euthanized by total blood sampling using anticoagulant (EDTA-2Na) and cervical dislocation under general anesthesia of inhalation by isoflurane. The whole blood was quickly placed on ice. Dissections were performed to harvest the liver tissues to measure the liver weight, and then the tissues for mitochondrial isolation were quickly placed on ice. The tissues were immersed in 10% Formalin Neutral Buffer Solution for to make FFPE tissue blocks and they were immersed into liquid nitrogen for the other analyses. The whole blood was centrifuged at 1,000g for 10 min at 4°C, and then aliquots of the plasmas were harvested and stored at -80°C for further analyses.

4.2. Mitochondrial isolation

Mitochondria in the liver tissues were isolated according to the method reported by Clayton DA and Shadel GS [47] with minor modifications as follows: 1x MS homogenization buffer containing 210 mM mannitol, 70 mM sucrose, 5 mM Tris-HCl (pH 7.5), 1 mM EDTA (pH 7.5), 1 mM dithiothreitol and protease inhibitor cocktail (Cat# 25955-24; Nacalai Tesque, Nakagyo, Kyoto, Japan) were applied to the tissues. Then, the liver tissues were homogenized with a buffer (μ l): tissue (mg) ratio of 10:1, using Potter-Elvehjem tissue grinders on ice. After that, the homogenates were centrifuged in 1,300xg at 4°C for 10 min. The supernatant of 500 μ l was placed in a new micro tube, centrifugation was again performed at 12,000 x g at 4°C for 15min, which produced the mitochondrial pellet. After the centrifugation and removal of the supernatant, the mitochondrial pellet was suspended in 500 μ l of the 1x MS homogenization buffer and again centrifuged in 12,000xg at 4°C for 15 min (the wash step). After that the washed mitochondrial pellets were suspended in 500 μ l of PBS and subjected to further analysis. In the ND group, the experimental procedure failed in one sample, which became N=11 in the analysis using isolated mitochondria.

4.3. Measurements of general markers in the plasma

General plasma biomarkers of ALT (IU/L), AST (IU/L), NEFFA (μ Eq/L), T-CHO (mg/dL), HDL (mg/dL), and LDL (mg/dL) in the plasma were measured by the Oriental Yeast Co., ltd. (Itabashi, Tokyo, Japan) as outsourcing. Plasma TG (mg/dL) was measured as duplicate measurements using a LabAssay Triglyceride kit (FUJIFILM Wako Pure Chemical Corporation, Osaka, Osaka, Japan) according to the manufacturer's instructions.

4.4. Tissue staining

The FFPE block of the liver was sectioned at a thickness of 4 μ m. The sections were placed on glass slides and subjected to HE and MT staining using Mayer's Hematoxylin Solution and 1% Eosin Y Solution (Muto Pure Chemicals, Bunkyo, Tokyo, Japan) for HE staining, and Aniline Blue Solution, Masson Stain Solution B, 0.75% Orange G Solution and 2.5% Phosphotungstic Acid Solution (Muto Pure Chemicals) for the MT stain. The staining protocols followed the manufacturer's instructions of the Muto Pure Chemicals. After staining, their morphology was examined under a model BZ-X710 microscope (Keyence, Osaka, Osaka, Japan) to assess the lipid droplets, inflammatory findings, and degree of fibrosis. The lipid droplet areas (%) of the entire image were quantified in 3 different places on the same sections stained by HE, as triplicate measurements in ImageJ Fiji (ver. Java 8).

The SAF scoring system to evaluate the pathology of NAFLD was also applied to the stained tissues, according to the previous research [22]. This evaluation was performed by a clinical technologist and medical doctor, in duplicate measurements.

IF staining was also conducted to assess the localization signals on the cell accumulation site. The sections on the slide glass were deparaffinized and hydrated. After that, the sections were placed in 0.01 M citrate buffer (pH 6.0) and subjected to antigen activation at 121°C for 10 min. Then, the sections were gently washed with phosphate buffered saline (PBS) for 10 min 3 times, and blocked with 5% skim milk/0.3% Triton X-100/PBS (PBS-T) for 1 hour at room temperature. After that, they were washed 3 times with PBS for 10 min each, then incubated with the primary antibodies rabbit anti-myeloperoxidase (Cat#EPR20257; Abcam, Cambridge, UK) and mouse anti- α -tubulin (Cat#66031-1-Ig; Proteintech, Rosemont, IL, USA) diluted at 1:100 in 1% BSA/PBS-T in a wet box at 4°C overnight. After washing three times with PBS for 10 min each time, the secondary antibodies goat anti-mouse IgG, FITC conjugate (Cat# SA00003-1; Proteintech) and goat anti-rabbit IgG, TRITC conjugate (Cat# SA00007-2; Proteintech) diluted at 1:100 in 1% BSA/PBS-T buffer were applied to the sections and they were incubated in a wet box at room temperature for 1 hour. After washing three times in PBS for 10 min each, mounting medium with DAPI (Dapi-Fluoromount-G; Cat#0100-01; SouthernBiotech, Birmingham, AL, USA) was applied to the sections and they were sealed with a cover glass. The morphology was examined under a model BZ-X710 microscope (Keyence) to assess localizations of the nucleus and myeloperoxidase.

4.5. Measurements of TG in the liver

To extract the lipids, the Folch method [48] was performed on the liver tissues by reference to the textbook [49] with some modifications. The liver tissues were homogenized in Milli-Q water (Merck Millipore, Burlington, MA, USA) at a ratio of 1:10 (tissue mg:Milli-Q water μ L) with zirconia beads, then 440 μ l of the homogenates were transferred to new micro tubes containing 1.1 mL chloroform-methanol solution (ratio 2:1). After shaking violently, centrifugation was performed at 15,000xg at 4°C for 5 min. After that, 400 μ L of the lower organic layer was transferred to a new micro tube, then the solutions were incubated to volatilize on a heat bloc at 80°C for 10 min. The extracted lipid was dissolved to 100 μ L of 5% BSA/0.05% Triton-x/PBS buffer with sonication. After that, TG (mg/dL) was measured by a LabAssay Triglyceride kit (FUJIFILM Wako Pure Chemical Corporation) using lipid samples of 5 μ l as duplicate measurements. Finally, the quantified values were converted to TG mg/g liver.

4.6. TBARS assay

The TBARS assay to measure lipid peroxidation in the liver tissues was performed according to the method previously reported by Kikugawa [50] with some modifications. First, the TBARS reaction mixture was made by adding the followed solutions to one bottle: 2 ml of 5.2% sodium dodecyl sulfate (SDS) in MilliQ water, 15 mL of 0.8% solution of thiobarbituric acid (TBA) in Milli-Q Water, 19.125 ml of MilliQ water alone, 500 μ l of 0.8% solution of butylated hydroxytoluene (BHT) in glacial acetic acid, and 8 mL of 0.1 M acetate buffer (pH 3.5). Then, the total volume of the mixture was 42.75 mL. After that, the TBARS mixture and liver tissues were mixed at a ratio of 9:1 (TBARS mixture μ l:liver mg) in a micro tube, then the tissues were homogenized under a beads crusher with zirconia beads. We transferred 500 μ l of the homogenate to a new micro tube and the samples were incubated at 4°C for one hour, followed by incubation at 95°C for one hour. After cooling the samples to room temperature, 500 μ L of 15:1 v/v 1-butanol and pyridine was added to the chilled tubes, and they were shaken. After that, the mixtures were centrifuged at 3,000 rpm for 10 min at 4°C. The fluorescence of the supernatant was measured at 540 nm excitation and 590 nm emission. The TBARS concentrations (nmol/mL) were calculated from a regression equation plotted with a 1,1,3,3-tetraethoxypropane standard (200 to 0.4

nmol/mL). Finally, the quantified values were converted to TBARS nmol/g liver. This assay was conducted in duplicate measurements.

4.7. DCF assay

DCF assays to measure the production of free radicals in the liver were performed by referring to the method reported by Ali et al. [51], Puntel et al. [52] and Sugasawa et al. [53] with some modifications, adapted to the liver homogenate. First, the liver tissues (approximately 100 mg) were homogenized with a beads crusher in protein lysis buffer (1% NP40, 150 mM NaCl, 50 mM Tris-HCl [pH 7.5]) including a protease inhibitor cocktail (Cat# 25955-24; Nacalai Tesque) in a micro tube. Then, the homogenates were centrifuged 12,000xg at 4°C for 15 min. After that, supernatants of the protein lysate were transferred to new micro tubes and the protein concentrations were measured using a BCA assay kit (Cat#RR036A, Takara Bio, Kusatsu, Shiga, Japan) according to the manufacture's instructions. After dilution and adjusting the protein lysate to 0.1 mg/mL protein, 10 μ l of the protein lysate was mixed with 100 μ l of 10 mM Tris-HCl (pH 7.4) containing 5 μ M 2',7'-dichlorodihydrofluorescein diacetate (DCFH-DA) in a black microplate well. After incubating this plate at 37°C for 60 min, the fluorescence intensity of the solution at 525 nm was measured in duplicate by irradiating it with excitation light at 488 nm. The DCF concentrations were calculated from a regression equation plotted with a DCF standard (200 to 6.25 pmol/mL). Finally, the quantified values were normalized as DCF pmol/mg protein. This assay was conducted using duplicate measurements.

4.8. CAT assay

A CAT assay to measure catalase activity was performed according to the published method by Sigma-Aldrich (St. Louis, MO, USA) [54] with some modifications. First, 10 μ l of the adjusted protein lysate (0.1 mg/mL), the same as in the DCF assay (section 4.7.), was mixed with 200 μ l of 50 mM potassium phosphate buffer (pH 7.0) containing 50 mM H₂O₂ in a UV micro plate, then its absorbance at 240 nm was immediately measured in a microplate reader (0 min). After that, the absorbance at 240 nm was again measured following incubation at room temperature for 10 min. The standard enzyme solution of catalase was also read on the same plate and time. Δ Absorbance as 0 min-10 min was calculated, and then the catalase activity (U/mL) was calculated from a regression equation plotted with the catalase activities standard (10-0.16 U/mL). Finally, the quantified values were normalized as CAT U/mg protein. This assay was conducted in duplicate measurements.

4.9. SOD assay

A SOD assay to measure the total SOD activity was performed according to the method previously reported by AV Peskin and CC Winterbourn [55] with some modifications. First, the following solutions were made: assay buffer with 50 mM sodium phosphate buffer (pH 8.0), containing 0.1mM diethylenetriaminepentaacetic acid (DTPA) and 0.1mM hypoxanthine; 10 mM WST-1 (DOJINDO, Mashiki, Kumamoto, Japan) in MilliQ water; catalase (FUJIFILM Wako Pure Chemical Corporation) 2 mg/ml in 50% glycerol; and xanthine oxidase (FUJIFILM Wako Pure Chemical Corporation) 13.8 mg /ml in 50% glycerol. Just before the assay, 20 mL of reaction mixture-1 was made as follows: 19.88 mL assay buffer/100 μ l WST-1 solution/20 μ l catalase solution. Also, 2 ml of the reaction mixture-2 was made as 1.98 mL assay buffer/20 μ l xanthine oxidase solution. Next, 10 μ l of the adjusted protein lysate (0.1 mg/mL), the same as in the DCF assay (section 4.7.), was applied to wells containing 200 μ l of the reaction mixture-1 in 96 well clear microplates. After that, reaction mixture-2 was also applied to the wells and mixed, followed by incubation at 37°C for 20 min. Standard samples to make a standard curve of the SOD activity were also reacted in same time and way. After the incubation, the absorbance at 450 nm referenced at 600 nm was measured in a microplate reader. Using the standard curve, the SOD activity (U/mL) of each sample was calculated. Finally, the quantified values were normalized as SOD U/mg protein. This assay was conducted in duplicate measurements.

4.10. Resazurin assay for the mitochondria

The Resazurin assay to measure mitochondrial activity was performed by referring to the method reported by Zhang HX et al. [56] and James FE et al. [57] with some modifications, adapted to the isolated mitochondria from the liver tissues. This assay has been considered able to measure the metabolic activity of mitochondrial respiration and the citric acid cycle [56, 57] because Resazurin can react with nicotinamide adenine dinucleotide (NADH) and can be structural changed as a fluorescence dye to Resorufin. First, Resazurin solution was added to a general cell culture medium (DMEM/high glucose, continuing antibiotics and 10% FBS) to a concentration of 100 μ M to prepare the reaction medium. Then, 20 μ l of isolated mitochondrial suspension, intact mitochondria from the liver, in PBS were applied to wells containing 200 μ l of the reaction medium in a 96 well clear microplate. After mixing well by pipetting, the plate was incubated in a CO₂ incubator (5% CO₂, 37°C, 100% humidity) for 3 hours. After the incubation, 100 μ l of the reaction samples were transferred to a 96 well black plate, then the fluorescence intensity was measured at 530 nm excitation and 590 nm emission in a microplate reader. Finally, the quantified values were converted to Resorufin fluorescence/mg liver. This assay was conducted as triplicate measurements.

4.11. JC-1 assay for the mitochondria

The JC-1 assay to measure mitochondrial activity was performed by referring to the method reported by Sugawara et al. [53] with some modifications, adapted to the isolated mitochondria from the liver tissues. First, JC-1 (PromoKine, Heidelberg, DER) dissolved in DMSO was added to a general cell culture medium (DMEM/high glucose, continuing antibiotics and 10%FBS) to a concentration of 2 μ M to prepare the reaction medium. To make a pellet of the mitochondria, 100 μ l of the isolated mitochondrial suspension in a micro tube was centrifuged in 12,000 \times g at 4°C for 15 min; then, the pellet was resuspended in the reaction medium, followed by incubation at 37°C for 15 min. After washing with 1 ml of PBS, the stained pellet was suspended in Hank's Balanced Salt Solution with Mg²⁺ and then 100 μ l of the suspension was transferred to 96 well black plates. Subsequently, the fluorescent intensities at excitation of 535 nm/ emission of 595 nm (red fluorescence) were measured in a microplate reader. Finally, the quantified values were converted to JC-1 red fluorescence/mg liver. This assay was conducted in triplicate measurements.

4.12. Measurements of mtDNA copy numbers in the isolated mitochondria

First, 50 μ l of isolated mitochondrial suspension was mixed and vortexed with 50 μ l of 1% Triton-X/PBS continuing proteinase K (7 U/ml) to make a mitochondrial DNA lysate. The lysate was then incubated at 56°C for 10 min to degrade the protein, followed by incubation at 95°C for 10 min to inactivate the proteinase K. After that, the lysate was diluted 10-fold using Milli-Q Water. The diluted lysate as a template was subjected to quantitative real-time PCR (qPCR) by SYBR Green dye for absolute quantification of the mitochondrial DNA copy number targeting the *mtCox-1* gene body, using a standard curve. The primer sequences are shown as supplementary Table S1. Detailed conditions of the qPCR are described in section 4.15. Standard DNA fragments for the standard curve were prepared following gel extraction purification. After the qPCR, it was confirmed that the standard curve was R²=0.99. Finally, the quantified mitochondrial DNA (mtDNA) copy numbers were converted to mtDNA copy number/mg liver.

4.13. Measurements of the mtDNA copy numbers in the liver

To measure the mtDNA copy numbers normalized by genomic DNA (gDNA), total RNA were extracted from the liver tissues, using phenol/chloroform/isoamyl alcohol solution (Cat#25970-56; Nacalai Tesque,). The extraction was performed according to the manufacturer's instructions. The DNA pellet was dissolved in Milli-Q Water, the DNA concentration was adjusted to 20 ng/ μ l as the template for the qPCR. The qPCR assay

based on SYBR Green dye was performed to target the *mtCox-1* gene body and the gDNA sequence. The primer sequences are shown in supplementary Table S1. Detailed conditions of the qPCR are described in section 4.15. After the qPCR assay, mtDNA copy numbers normalized by gDNA (mtDNA/gDNA copy number) were calculated using threshold cycle (CT) values and the $2^{\Delta\Delta CT}$ method.

4.14. Gene expression analysis

To quantify gene expression of various markers in the liver and the whole blood, total RNA was extracted from the liver tissues 50-100 mg and whole blood of 100 μ l, using Sepasol-RNA I Super G (Cat# 09379-55; Nacalai Tesque.). The extraction was performed according to the manufacturer's instructions. The extracted total RNA solution in Milli-Q Water was diluted and adjusted to a concentration of 100 ng/ μ l. Then, 500 ng of RNA was used to make cDNAs with the PrimeScript RT Master Mix (Cat#RR036A, Takara Bio) according to the manufacturer's instructions. The cDNAs were diluted at $\times 10$ using Milli-Q Water and subjected to qPCR assay based on SYBR Green dye. The target genes were markers for inflammation, cell growth, fibrosis, antioxidative enzymes, NRF2 target genes (reflecting oxidative stress), lipogenesis, and gluconeogenesis. The primer sequences are shown in supplementary Table S1. Detailed conditions of the qPCR assay are described in section 4.15. After the qPCR assay, values of relative gene expression normalized by the *36B4* (*Rplp0*) gene were calculated using threshold cycle (CT) values and the $2^{\Delta\Delta CT}$ method.

4.15. qPCR assay

First, the reaction plate was prepared as follows: 2 μ L of template, 0.1 μ l of 10 μ M primer solution (forward and reverse each), 5 μ l of master mix (KAPA SYBR FAST qPCR Kits, Cat# KK4620; NIPPON Genetics, Bunkyo, Tokyo, Japan) and 2.8 μ l Milli-Q Water were included in a total reaction volume of 10 μ L per well on a qPCR plate. Negative control wells were also prepared by using MilliQ-Water in the assays instead of template. Then, the qPCR assay was performed on a QuantStudio 5 Real-Time PCR System (Thermo Fisher Scientific, Waltham, MA, USA) in thermal cycle conditions as follows: one cycle of 95°C for 5 min, followed by 40 cycles of 95°C for 3 s and 60°C for 30 s, with a final stage of melting curve analysis. All qPCR assays were conducted as duplicate measurements.

4.16. Western Blot analysis

First, the protein lysate of the whole liver, that is the same sample in the DCF assay (section 4.7.), was adjusted to a protein concentration of 2 mg/ml and the mitochondrial suspension, that is the same sample in section 4.2., was also prepared. The lysate or suspension were mixed with 2xloading buffer containing 2-mercaptoethanol and denatured at 95°C for 5 min. After this procedure, the samples to detect OXPHOS proteins were incubated at room temperature for 20 min instead of 95°C for 5 min because the OXPHOS proteins are very sensitive to high temperatures. The 10 μ l prepared samples were subjected sodium dodecyl sulfate polyacrylamide gel electrophoresis (SDS-PAGE) using 10 or 15% gels at 140 V for 70 min, and then the separated proteins in the gel were transferred to polyvinylidene fluoride (PVDF) membrane using a wet transfer method in 40 V at 4°C overnight. This membrane was blocked with TBS-T buffer (50 mM Tris-HCl, 150 mM NaCl, 0.05% Tween 20, pH 7.6) including 5% skim milk for 30 min, and then the membrane was washed with TBS-T buffer, 3 times for 10 min. Subsequently, the membrane was immersed in a properly diluted primary antibody and incubated with gentle shaking overnight at 4°C. After washing it with TBS-T buffer 3 times for 10 min, the membrane was immersed in a properly diluted secondary antibody and incubated with gentle shaking for 30 min at room temperature. After washing the membrane, the target protein bands were visualized with a chemiluminescence reagent (Amersham ECL Select, Cat# RPN2235; Cytiva, Shinjuku, Tokyo, Japan) on ImageQuant LAS 4000 (cytiva), followed by export as 16 bit TIFF images. The luminance of the bands of the TIFF images were quantified using ImageJ Fiji (ver. Java 8). Information about the antibodies is shown in

supplementary Table S2. Raw data of the WB analysis for all samples are provided as supplementary Figure S1.

4.17. Statistics

All data were statistically analyzed using GraphPad Prism version 9.0.2 (GraphPad, San Diego, CA, USA). First, for all experimental data, we conducted the Shapiro-Wilk normality test to check the normality of the distributions. Subsequently, we decided to use non-parametric tests for all data. Kruskal-Wallis H tests (one-way ANOVA of ranks) were also performed, followed by a two-stage Benjamini, Krieger, and Yekutieli False Discovery Rate (FDR) procedure as a post hoc test. A p value less than 0.05 was considered statistically significant. In the graphs, individual values were plotted with median and interquartile range. In some graphs, the y-axis is displayed logarithmically, because there are groups that show drastic changes of the values.

Supplementary Materials: The following are available online at www.mdpi.com/xxx/s1, Figure S1: raw data of WB analysis for all samples, Table S1: primer sequences used in this study, Table S2: information of the antibodies in the WB analysis.

Author Contributions: Conceptualization, methodology, validation, formal analysis, investigation, data curation, writing—original draft preparation, writing—review and editing, visualization, project administration, T.S., S.O. and M.Y.; formal analysis, investigation, writing—original draft preparation, writing—review and editing, S.F.; writing—original draft preparation, writing—review and editing, Y.M.; writing—review and editing, K.A., T.N., S.T. and Y.Y., writing—review and editing, supervision, Y.K and K.T. All authors have read and agreed to the published version of the manuscript.

Funding: Not applicable.

Institutional Review Board Statement: The study was conducted according to the guidelines (corporation regulation; No. 50, July 21, 2005) of the animal experiments by the Animal Ethics Committee of University of Tsukuba. The approval number was 20-133 (May 1, 2020).

Informed Consent Statement: Not applicable.

Data Availability Statement: Not applicable.

Conflicts of Interest: The authors declare no conflict of interest.

References

1. Huang, D. Q.; El-Serag, H. B.; Loomba, R. Global Epidemiology of NAFLD-Related HCC: Trends, Predictions, Risk Factors and Prevention. *Nat. Rev. Gastroenterol. Hepatol.* **2021**, *18* (4), 223–238. <https://doi.org/10.1038/s41575-020-00381-6>.
2. Kistler, K. D.; Molleston, J.; Unalp, A.; Abrams, S. H.; Behling, C.; Schwimmer, J. B. Symptoms and Quality of Life in Obese Children and Adolescents with Non-Alcoholic Fatty Liver Disease. *Aliment. Pharmacol. Ther.* **2010**, *31* (3), 396–406. <https://doi.org/10.1111/j.1365-2036.2009.04181.x>.
3. Newton, J. L. Systemic Symptoms in Non-Alcoholic Fatty Liver Disease. *Dig. Dis.* **2010**, *28* (1), 214–219. <https://doi.org/10.1159/000282089>.
4. Sarwar, R.; Pierce, N.; Koppe, S. Obesity and Nonalcoholic Fatty Liver Disease: Current Perspectives. *Diabetes, Metab. Syndr. Obes. Targets Ther.* **2018**, *11*, 533–542. <https://doi.org/10.2147/DMSO.S146339>.
5. National Institute of Diabetes and Digestive and Kidney Diseases (NIDDK), Treatment for NAFLD & NASH, How do doctors treat NAFLD and NASH? Available online: <https://www.niddk.nih.gov/health-information/liver-disease/nafl-d-nash/treatment> (accessed on 2 April 2021).
6. Siersbaek, M.; Varticovski, L.; Yang, S.; Baek, S.; Nielsen, R.; Mandrup, S.; Hager, G. L.; Chung, J. H.; Grøntved, L. High Fat Diet-Induced Changes of Mouse Hepatic Transcription and Enhancer Activity Can Be Reversed by Subsequent Weight Loss. *Sci. Rep.* **2017**, *7*, 28071704. <https://doi.org/10.1038/srep40220>.
7. Benard, O.; Lim, J.; Apontes, P.; Jing, X.; Angeletti, R. H.; Chi, Y. Impact of High-Fat Diet on the Proteome of Mouse Liver. *J. Nutr. Biochem.* **2016**, *31*, 10–19. <https://doi.org/10.1016/j.jnutbio.2015.12.012>.
8. Tsuru, H.; Osaka, M.; Hiraoka, Y.; Yoshida, M. HFD-Induced Hepatic Lipid Accumulation and Inflammation Are Decreased in Factor D Deficient Mouse. *Sci. Rep.* **2020**, *10* (1), 33067533. <https://doi.org/10.1038/s41598-020-74617-5>.
9. Purushotham, A.; Xu, Q.; Li, X. Systemic SIRT1 Insufficiency Results in Disruption of Energy Homeostasis and Steroid Hormone Metabolism upon High-fat-diet Feeding. *FASEB J.* **2012**, *26* (2), 656–667. <https://doi.org/10.1096/fj.11-195172>

10. Yu, J.; Yang, X.; Yang, X.; Yang, M.; Wang, P.; Yang, Y.; Yang, J.; Li, W.; Xu, J. Nonylphenol Aggravates Non-Alcoholic Fatty Liver Disease in High Sucrose-High Fat Diet-Treated Rats. *Sci. Rep.* **2018**, *8* (1), 29459774. <https://doi.org/10.1038/s41598-018-21725-y>.
11. Yang, P.; Wang, Y.; Tang, W.; Sun, W.; Ma, Y.; Lin, S.; Jing, J.; Jiang, L.; Shi, H.; Song, Z.; Yu, L. Western Diet Induces Severe Nonalcoholic Steatohepatitis, Ductular Reaction, and Hepatic Fibrosis in Liver CGI-58 Knockout Mice. *Sci. Rep.* **2020**, *10* (1), 32170127. <https://doi.org/10.1038/s41598-020-61473-6>.
12. Luo, Y.; Burrington, C. M.; Graff, E. C.; Zhang, J.; Judd, R. L.; Suksaranjit, P.; Kaewpoowat, Q.; Davenport, S. K.; O'Neill, A. M.; Greene, M. W. Metabolic Phenotype and Adipose and Liver Features in a High-Fat Western Diet-Induced Mouse Model of Obesity-Linked NAFLD. *Am. J. Physiol. - Endocrinol. Metab.* **2016**, *310* (6), E418–E439. <https://doi.org/10.1152/ajpendo.00319.2015>.
13. Hoffmann, C.; Djerir, N. E. H.; Danckaert, A.; Fernandes, J.; Roux, P.; Charrueau, C.; Lachagès, A. M.; Charlotte, F.; Brocheriou, I.; Clément, K.; Aron-Wisniewsky, J.; Foufelle, F.; Ratziu, V.; Hainque, B.; Bonnefont-Rousselot, D.; Bigey, P.; Escriou, V. Hepatic Stellate Cell Hypertrophy Is Associated with Metabolic Liver Fibrosis. *Sci. Rep.* **2020**, *10* (1), 32123215. <https://doi.org/10.1038/s41598-020-60615-0>.
14. Lu, Y.; Su, X.; Zhao, M.; Zhang, Q.; Liu, C.; Lai, Q.; Wu, S.; Fang, A.; Yang, J.; Chen, X.; Yao, Y. Comparative RNA-Sequencing Profiled the Differential Gene Expression of Liver in Response to Acetyl-CoA Carboxylase Inhibitor GS-0976 in a Mouse Model of NASH. *PeerJ* **2019**, *2019* (12), 31879571. <https://doi.org/10.7717/peerj.8115>.
15. Rokugawa, T.; Konishi, H.; Ito, M.; Iimori, H.; Nagai, R.; Shimosegawa, E.; Hatazawa, J.; Abe, K. Evaluation of Hepatic Integrin $\text{Av}\beta 3$ Expression in Non-Alcoholic Steatohepatitis (NASH) Model Mouse by 18F-FPP-RGD2 PET. *EJNMMI Res.* **2018**, *8* (1), 29855729. <https://doi.org/10.1186/s13550-018-0394-4>.
16. Ikawa-Yoshida, A.; Matsuo, S.; Kato, A.; Ohmori, Y.; Higashida, A.; Kaneko, E.; Matsumoto, M. Hepatocellular Carcinoma in a Mouse Model Fed a Choline-Deficient, L-Amino Acid-Defined, High-Fat Diet. *Int. J. Exp. Pathol.* **2017**, *98* (4), 221–233. <https://doi.org/10.1111/iepp.12240>.
17. Begriche, K.; Igoudjil, A.; Pessayre, D.; Fromenty, B. Mitochondrial Dysfunction in NASH: Causes, Consequences and Possible Means to Prevent It. *Mitochondrion* **2006**, *6* (1), 1–28. <https://doi.org/10.1016/j.mito.2005.10.004>.
18. Buzzetti, E.; Pinzani, M.; Tsochatzis, E. A. The Multiple-Hit Pathogenesis of Non-Alcoholic Fatty Liver Disease (NAFLD). *Metabolism*. **2016**, *65* (8), 1038–1048. <https://doi.org/10.1016/j.metabol.2015.12.012>.
19. Wang, J.; Wang, J.; He, W.; He, W.; Tsai, P. J.; Chen, P. H.; Ye, M.; Guo, J.; Su, Z. Mutual Interaction between Endoplasmic Reticulum and Mitochondria in Nonalcoholic Fatty Liver Disease. *Lipids Health Dis.* **2020**, *19* (1), 32284046. <https://doi.org/10.1186/s12944-020-01210-0>.
20. Nelson, J. E.; Klintworth, H.; Kowdley, K. V. Iron Metabolism in Nonalcoholic Fatty Liver Disease. *Curr. Gastroenterol. Rep.* **2012**, *14* (1), 8–16. <https://doi.org/10.1007/s11894-011-0234-4>.
21. Giorgio, V.; Prono, F.; Graziano, F.; Nobili, V. Pediatric Non Alcoholic Fatty Liver Disease: Old and New Concepts on Development, Progression, Metabolic Insight and Potential Treatment Targets. *BMC Pediatr.* **2013**, *13* (1), 23530957. <https://doi.org/10.1186/1471-2431-13-40>.
22. Bedossa, P.; Poitou, C.; Veyrie, N.; Bouillot, J. L.; Basdevant, A.; Paradis, V.; Tordjman, J.; Clement, K. Histopathological Algorithm and Scoring System for Evaluation of Liver Lesions in Morbidly Obese Patients. *Hepatology* **2012**, *56* (5), 1751–1759. <https://doi.org/10.1002/hep.25889>.
23. Pérez-Carreras, M.; Del Hoyo, P.; Martín, M. A.; Rubio, J. C.; Martín, A.; Castellano, G.; Colina, F.; Arenas, J.; Solis-Herruzo, J. A. Defective Hepatic Mitochondrial Respiratory Chain in Patients with Nonalcoholic Steatohepatitis. *Hepatology* **2003**, *38* (4), 999–1007. <https://doi.org/10.1053/jhep.2003.50398>.
24. Musolino, V.; Gliozzi, M.; Scarano, F.; Bosco, F.; Scicchitano, M.; Nucera, S.; Carresi, C.; Ruga, S.; Zito, M. C.; Maiuolo, J.; Macrì, R.; Amodio, N.; Juli, G.; Tassone, P.; Mollace, R.; Caffrey, R.; Marioneaux, J.; Walker, R.; Ehrlich, J.; Palma, E.; Muscoli, C.; Bedossa, P.; Salvemini, D.; Mollace, V.; Sanyal, A. J. Bergamot Polyphenols Improve Dyslipidemia and Pathophysiological Features in a Mouse Model of Non-Alcoholic Fatty Liver Disease. *Sci. Rep.* **2020**, *10* (1), 32054943. <https://doi.org/10.1038/s41598-020-59485-3>.
25. Nascimbeni, F.; Bedossa, P.; Fedchuk, L.; Pais, R.; Charlotte, F.; Lebray, P.; Poynard, T.; Ratziu, V. Clinical Validation of the FLIP Algorithm and the SAF Score in Patients with Non-Alcoholic Fatty Liver Disease. *J. Hepatol.* **2020**, *72* (5), 828–838. <https://doi.org/10.1016/j.jhep.2019.12.008>.
26. Ipsen, D. H.; Lykkesfeldt, J.; Tveden-Nyborg, P. Molecular Mechanisms of Hepatic Lipid Accumulation in Non-Alcoholic Fatty Liver Disease. *Cell. Mol. Life Sci.* **2018**, *75* (18), 3313–3327. <https://doi.org/10.1007/s00018-018-2860-6>.
27. Serviddio, G.; Bellanti, F.; Tamborra, R.; Rollo, T.; Capitanio, N.; Romano, A. D.; Sastre, J.; Vendemiale, G.; Altomare, E. Uncoupling Protein-2 (UCP2) Induces Mitochondrial Proton Leak and Increases Susceptibility of Non-Alcoholic Steatohepatitis (NASH) Liver to Ischaemia-Reperfusion Injury. *Gut* **2008**, *57* (7), 957–965. <https://doi.org/10.1136/gut.2007.147496>.
28. Zhiming, W. U.; Wang, H.; Fang, S.; Xu, C. Roles of Endoplasmic Reticulum Stress and Autophagy on H₂O₂-induced Oxidative Stress Injury in HepG2 Cells. *Mol. Med. Rep.* **2018**, *18* (5), 4163–4174. <https://doi.org/10.3892/mmr.2018.9443>.
29. Videla, L. A.; Rodrigo, R.; Orellana, M.; Fernandez, V.; Tapia, G.; Quiñones, L.; Varela, N.; Contreras, J.; Lazarte, R.; Csendes, A.; Rojas, J.; Maluenda, F.; Burdiles, P.; Diaz, J. C.; Smok, G.; Thielemann, L.; Poniachik, J. Oxidative Stress-Related Parameters in the Liver of Non-Alcoholic Fatty Liver Disease Patients. *Clin. Sci.* **2004**, *106* (3), 261–268. <https://doi.org/10.1042/CS20030285>.
30. Ighodaro, O. M.; Akinloye, O. A. First Line Defence Antioxidants-Superoxide Dismutase (SOD), Catalase (CAT) and Glutathione Peroxidase (GPX): Their Fundamental Role in the Entire Antioxidant Defence Grid. *Alexandria J. Med.* **2018**, *54* (4), 287–293. <https://doi.org/10.1016/j.ajme.2017.09.001>.

31. Nassir, F.; Ibdah, J. A. Role of Mitochondria in Nonalcoholic Fatty Liver Disease. *Int. J. Mol. Sci.* **2015**, *15* (5), 8713–8742. <https://doi.org/10.3390/ijms15058713>.
32. Simões, I. C. M.; Fontes, A.; Pinton, P.; Zischka, H.; Wieckowski, M. R. Mitochondria in Non-Alcoholic Fatty Liver Disease. *Int. J. Biochem. Cell Biol.* **2018**, *95*, 93–99. <https://doi.org/10.1016/j.biocel.2017.12.019>.
33. Dornas, W.; Schuppan, D. Mitochondrial Oxidative Injury: A Key Player in Nonalcoholic Fatty Liver Disease. *Am. J. Physiol. - Gastrointest. Liver Physiol.* **2020**, *319* (3), G400–G411. <https://doi.org/10.1152/AJPGI.00121.2020>.
34. Berson, A.; De Beco, V.; Letteron, P.; Robin, M. A.; Moreau, C.; El Kahwaji, J.; Verthier, N.; Feldmann, G.; Fromenty, B.; Pessayre, D. Steatohepatitis-Inducing Drugs Cause Mitochondrial Dysfunction and Lipid Peroxidation in Rat Hepatocytes. *Gastroenterology* **1998**, *114* (4 I), 764–774. [https://doi.org/10.1016/S0016-5085\(98\)70590-6](https://doi.org/10.1016/S0016-5085(98)70590-6).
35. Kaushal, G.P.; Chandrashekar, K.; Juncos, L.A. Molecular Interactions Between Reactive Oxygen Species and Autophagy in Kidney Disease. *Int. J. Mol. Sci.* **2019**, *20*, 3791. <https://doi.org/10.3390/ijms20153791>
36. Song, J. Y.; Shen, T. C.; Hou, Y. C.; Chang, J. F.; Lu, C. L.; Liu, W. C.; Chen, P. J.; Chen, B. H.; Zheng, C. M.; Lu, K. C. Influence of Resveratrol on the Cardiovascular Health Effects of Chronic Kidney Disease. *Int. J. Mol. Sci.* **2020**, *21* (17), 1–16. <https://doi.org/10.3390/ijms21176294>.
37. Sandoval-Acuña, C.; Ferreira, J.; Speisky, H. Polyphenols and Mitochondria: An Update on Their Increasingly Emerging ROS-Scavenging Independent Actions. *Arch. Biochem. Biophys.* **2014**, *559*, 75–90. <https://doi.org/10.1016/j.abb.2014.05.017>.
38. Younossi, Z. M.; Koenig, A. B.; Abdelatif, D.; Fazel, Y.; Henry, L.; Wymer, M. Global Epidemiology of Nonalcoholic Fatty Liver Disease—Meta-Analytic Assessment of Prevalence, Incidence, and Outcomes. *Hepatology* **2016**, *64* (1), 73–84. <https://doi.org/10.1002/hep.28431>.
39. Byrne, C. D.; Targher, G. NAFLD: A Multisystem Disease. *J. Hepatol.* **2015**, *62* (S1), S47–S64. <https://doi.org/10.1016/j.jhep.2014.12.012>.
40. Sobhonslidsuk, A.; Jongjirasiri, S.; Thakkinian, A.; Wisedopas, N.; Bunnag, P.; Puavilai, G. Visceral Fat and Insulin Resistance as Predictors of Non-Alcoholic Steatohepatitis. *World J. Gastroenterol.* **2007**, *13* (26), 3614–3618. <https://doi.org/10.3748/wjg.v13.i26.3614>.
41. Mansour-Ghanaei, R.; Mansour-Ghanaei, F.; Naghipour, M.; Joukar, F. Biochemical markers and lipid profile in nonalcoholic fatty liver disease patients in the PERSIAN Guilan cohort study (PGCS), Iran. *J Family Med Prim Care.* **2019**, *8*(3), 923–928. https://doi:10.4103/jfmpc.jfmpc_243_18.
42. Fabbrini, E.; Sullivan, S.; Klein, S. Obesity and Nonalcoholic Fatty Liver Disease: Biochemical, Metabolic, and Clinical Implications. *Hepatology.* **2010**, *51* (2), 679–689. <https://doi.org/10.1002/hep.23280>.
43. Yasuda, D.; Torii, H.; Shimizu, R.; Hiraoka, Y.; Kume, N. Reduced Serum Cholesterol and Triglyceride Levels in a Choline-Deficient L-Amino Acid-Defined High-Fat Diet (CDAHFD)-Induced Mouse Model of Non-Alcoholic Steatohepatitis (NASH). *Biol. Pharm. Bull.* **2020**, *43* (4), 616–618. <https://doi.org/10.1248/bpb.b19-00338>.
44. Sudoh, M.; Matsumoto, M. An Approach for Anti-Fibrotic Drug Discovery in NASH. *Folia Pharmacol. Jpn.* **2014**, *144* (2), 69–74. <https://doi.org/10.1254/fpj.144.69>.
45. Zhang, Z.; Wang, X.; Zheng, G.; Shan, Q.; Lu, J.; Fan, S.; Sun, C.; Wu, D.; Zhang, C.; Su, W.; Sui, J.; Zheng, Y. Troxerutin Attenuates Enhancement of Hepatic Gluconeogenesis by Inhibiting NOD Activation-Mediated Inflammation in High-Fat Diet-Treated Mice. *Int. J. Mol. Sci.* **2017**, *18* (1), 28029143. <https://doi.org/10.3390/ijms18010031>.
46. Okin, D.; Medzhitov, R. The Effect of Sustained Inflammation on Hepatic Mevalonate Pathway Results in Hyperglycemia. *Cell* **2016**, *165* (2), 343–356. <https://doi.org/10.1016/j.cell.2016.02.023>.
47. Clayton, D. A.; Shadel, G. S. Isolation of Mitochondria from Animal Tissue. *Cold Spring Harb. Protoc.* **2014**, *2014* (10), 1112–1114. <https://doi.org/10.1101/pdb.prot080010>.
48. Folch, J.; Lees, M.; Sloane, S. G. A simple method for the isolation and purification of total lipides from animal tissues. *J Biol Chem.* **1957**, *226*(1), 497–509.
49. Yoshikawa, H. Extraction and quantification of liver lipid. In *An Introduction to Practical Biochemistry*, 1st ed.; Tashiro, M., Eds.; Kagaku-Dojin Publishing Company: Shimogyo, Kyoto, Japan, 2007; Volume 5, pp. 43–44.
50. Kikugawa, K.; Yasuhara, Y.; Ando, K.; Koyama, K.; Hiramoto, K.; Suzuki, M. Effect of Supplementation of N-3 Polyunsaturated Fatty Acids on Oxidative Stress-Induced DNA Damage of Rat Hepatocytes. *Biol. Pharm. Bull.* **2003**, *26* (9), 1239–1244. <https://doi.org/10.1248/bpb.26.1239>.
51. Ali, S.F.; LeBel, C.P.; Bondy, S.C. Reactive oxygen species formation as a biomarker of methylmercury and trimethyltin neurotoxicity. *Neurotoxicology.* **1992**, *13*(3), 637–648.
52. Puntel, G. O.; Carvalho, N. R.; Dobrachinski, F.; Salgueiro, A. C. F.; Puntel, R. L.; Folmer, V.; Barbosa, N. B. V.; Royes, L. F. F.; Rocha, J. B. T.; Soares, F. A. A. Cryotherapy Reduces Skeletal Muscle Damage after Ischemia/Reperfusion in Rats. *J. Anat.* **2013**, *222* (2), 223–230. <https://doi.org/10.1111/joa.12009>.
53. Sugawara, T.; Mukai, N.; Tamura, K.; Tamba, T.; Mori, S.; Miyashiro, Y.; Yamaguchi, M.; Nissato, S.; Ra, S.; Yoshida, Y.; Hoshino, M.; Ohmori, H.; Kawakami, Y.; Takekoshi, K. Effects of Cold Stimulation on Mitochondrial Activity and VEGF Expression in Vitro. *Int. J. Sports Med.* **2016**, *37* (10), 766–778. <https://doi.org/10.1055/s-0042-102659>.
54. Sigma-Aldrich, Enzymatic Assay of Catalase (EC 1.11.1.6). Available online: <https://www.sigmaaldrich.com/technical-documents/protocols/biology/enzymatic-assay-of-catalase.html> (accessed on 12 April 2021).
55. Peskin, A. V.; Winterbourn, C. C. A Microtiter Plate Assay for Superoxide Dismutase Using a Water-Soluble Tetrazolium Salt (WST-1). *Clin. Chim. Acta* **2000**, *293* (1–2), 157–166. [https://doi.org/10.1016/S0009-8981\(99\)00246-6](https://doi.org/10.1016/S0009-8981(99)00246-6).
56. Zhang, H.; Du, G.; Zhang, J. Assay of Mitochondrial Functions by Resazurin in Vitro. *Acta Pharmacol. Sin.* **2004**, *25* (3), 385–389.

-
57. Grey, J. F. E.; Townley, A. R.; Everitt, N. M.; Campbell-Ritchie, A.; Wheatley, S. P. A Cost-Effective, Analytical Method for Measuring Metabolic Load of Mitochondria. *Metab. Open* **2019**, *4*, 100020. <https://doi.org/10.1016/j.metop.2019.100020>.